Mating of active particles in turbulent flows

By R. Chang† AND R. Chajwa†

Marine plankton live in a turbulent ocean, where active particles can condense onto singular, low-dimensional manifolds, known as caustics, that can drastically enhance encounter rates (Chajwa *et al.* 2023). Thus, the ecological dynamics lies mostly on these extremal curves and surfaces in two and three dimensions, respectively, but the ecological consequences of these singularities remain unexplored. Here, we endow the framework of active suspensions in flows with simple reproduction and death rules. We construct a particle-based model for replicating and dying swimmers coupled to two-dimensional turbulence solved using pseudospectral direct numerical simulation (DNS). Each swimmer dies at a fixed rate and reproduces when it encounters another within a prescribed distance. In the single-gender system, caustic formation concentrates swimmers into dense bands, sustaining the population. In the two-gender system, reproduction succeeds only when both genders form overlapping caustics. Even small motility differences misalign the extremal structures, suppress encounters, and cause population collapse. These results demonstrate that turbulence- and motility-driven caustics can dramatically alter replication and impose rigid constraints on motility synchrony between mating types, formally linking turbulence and eco-physiological adaptations in marine microbial systems.

1. Introduction

The vast and highly dilute nature of the ocean makes the ability of marine phytoplankton to find resources and one another a critical step in their life cycle. At microscopic scales, ecological processes are constrained by encounter rates, which govern predator–prey interactions, infection, and sexual reproduction (Menden-Deuer 2006; Kiørboe 2008). For species that rely on sexual reproduction, such as corals, copepods, and phytoplankton that alternate between sexual and asexual modes, the encounter of potential mates is often the bottleneck for long-term population persistence (Seuront & Stanley 2014). Understanding the physical and biological mechanisms that regulate encounters in the ocean is therefore central to ecological models and to predicting how populations respond to changing marine environments.

Many studies have examined behavioral adaptations that enhance encounter rates. For example, copepods are known to release pheromone trails to attract partners for reproduction (Kiørboe & Bagøien 2005). However, most of these observations were made in a static laboratory environment, where trails remain coherent (Yen & Lasley 2010; Bagøien & Kiørboe 2005). In the open ocean, turbulence dominates and constantly generates stretching and folding that rapidly distort and mix chemical signals. Whether pheromone trails or chemotaxis-based mechanisms remain effective for mating under turbulent flow is unknown.

To evaluate the feasibility of a chemotaxis-based mechanism for finding mates in the open ocean, we use *Chlamydomonas reinhardtii*, a model green alga, as an example for a

† The authors contributed equally to this work.

back-of-the-envelope analysis. *Chlamydomonas* has a radius of $a \approx 5$ μm and swims at $v \approx 100$ μm/s (Seed & Tomkins 2018). The density ratio is approximately 1.1, consistent with typical values reported for eukaryotic cells (Bryan *et al.* 2010). Small signaling molecules diffuse with $D_c \approx 10^{-9}$ m^2/s (Evans *et al.* 2018), and in the upper mixed layer the turbulence dissipation rate is $\epsilon = 10^{-8}$–10^{-6} m^2/s^3 with kinematic viscosity $\nu \approx 10^{-6}$ m^2/s (Guasto *et al.* 2012). Under these conditions, the Batchelor scale is $\ell_B = (\nu D_c^2/\epsilon)^{1/4} = 30$–$300$ μm, which represents the smallest length scale at which chemical gradients can persist. Turbulence sharpens gradients down to the Batchelor scale, but below ℓ_B diffusion erases them (Guasto *et al.* 2012). *Chlamydomonas* chemotaxis operates through the temporal integration of concentration changes rather than instantaneous surface comparison (Nelson *et al.* 2023). For pheromone concentrations of order 1 pM (Frenkel *et al.* 2014) and an integration time $T_i \sim 4$ s (Segall *et al.* 1986), the Berg–Purcell limit yields a fractional sensing error of $\delta c/\bar{c} = 1/\sqrt{D_c a \bar{c} T_i} \approx 0.29$, corresponding to a signal-to-noise ratio of only 3.4 in quiescent fluid (Berg & Purcell 1977). In turbulence, the Kolmogorov time $\tau_\eta = (\nu/\epsilon)^{1/2} \sim 1$–$10$ s (Guasto *et al.* 2012) is comparable to the integration time, so gradients decorrelate on the same timescale on which cells attempt to measure them. As a result, once two cells are separated by more than $\ell_B \sim 30$–300 μm, the chemical signal becomes homogenized before it can be resolved. This analysis suggests that chemotaxis is at best a short-range strategy for mate finding and, in turbulent flow, is unlikely to provide a reliable mechanism for encounters.

Although turbulence can limit the chemotaxis-based mechanism to a short range, turbulence itself may provide an alternative mechanism for encounters. For example, inertial particles suspended in turbulent flows are known to form singular structures called caustics. Caustics are singularities in the particle phase-space manifold where trajectories with different velocities converge to the same spatial location (Gustavsson *et al.* 2012). In configuration space, this process leads to sharply folded particle sheets and regions of formally infinite concentration, analogous to the bright curves of light formed when rays focus through a curved surface in optics. Unlike ordinary clustering, caustics are characterized by locally divergent density, multivalued velocity fields, and elevated collision rates (Papoutsakis & Gavaises 2020; Bhatnagar *et al.* 2022). In the context of turbulence, these focal surfaces arise when inertia allows particles to detach from the local fluid flow and cross streamlines. The result is a multivalued velocity field, where several particle velocities coexist at the same spatial point and the local collision and encounter rates increase dramatically. This mechanism is thought to underlie phenomena ranging from the rapid coalescence of water droplets in clouds (Bhatnagar *et al.* 2022) to planet formation (Pumir & Wilkinson 2016).

Recently, active particles driven by internal propulsion were demonstrated to form caustics in turbulent flows, where activity and shear interact to create transient, band-like structures (Chajwa *et al.* 2023). The regime boundaries for caustic formation have been mapped out in phase diagrams, identifying thresholds and limits in activity where caustics emerge. However, the biological implications of caustic formation remain poorly understood. In particular, it remains unclear whether caustics can directly regulate reproductive encounters in populations that rely on mating. To date, no study has asked whether caustics can sustain population growth under turbulent flow by amplifying mate encounters, or how mismatches in motility across genders affect the mating process.

In this work, we address this gap by combining a particle-based model of plankton reproduction with DNS of two-dimensional turbulence. We implement simple reproduction and death rules, in which particles die at a constant rate and reproduction occurs

when two compatible individuals approach within a threshold distance. We show that, in same-gender populations, caustics concentrate particles into transient bands that enable rapid population growth, whereas in their absence populations collapse. In cross-gender mating, reproduction succeeds only when caustics of both genders overlap. Mismatched caustics suppress encounters and lead to collapse despite the presence of caustics in each gender individually. These results indicate a new link between fluid mechanical singularities and reproductive dynamics, showing that caustic synchrony may be a prerequisite for sustained mating in turbulent flows.

2. Dynamical equations

The two-dimensional dynamics of the fluid is captured using a vorticity ω and stream function ψ formulation of the Navier–Stokes equation. In the Fourier space with wave vector $\mathbf{q} = (q_x, q_y)$, the fluid equations become

$$\tilde{\psi} = -\frac{\tilde{\omega}}{q^2}, \tag{2.1a}$$

$$\frac{\partial \tilde{\omega}}{\partial t} = i(q_x \widetilde{u_x \omega} + q_y \widetilde{u_y \omega}) - (\nu q^2 + \gamma)\tilde{\omega} + \tilde{f}, \tag{2.1b}$$

where $\tilde{\cdot}$ denotes Fourier-transformed variables, $(u_x, u_y) = (-\partial\psi/\partial y, \partial\psi/\partial x)$ is the flow velocity, ν is the kinematic velocity, γ is the Ekman friction (Boffetta & Ecke 2012), and f is the external forcing. We consider the forcing of the form $F_0 q_0 \cos q_0 x$ with the wave number q_0.

The active particles without inertia in two-dimensional turbulent flow are modeled as active Hookean dimers with a preferred extension w_0. The dynamical equations for the particle position $\mathbf{X}$ and extension $\mathbf{w}$ are

$$\dot{\mathbf{X}} = \mathbf{U} + \beta \mathbf{w}, \tag{2.2a}$$

$$\dot{\mathbf{w}} = \frac{1}{\tau}\left(1 - \frac{|\mathbf{w}|^2}{w_0^2}\right)\mathbf{w} + (\alpha \mathbf{S} + \mathbf{A}) \cdot \mathbf{w} - \ell^2 \nabla^2 \mathbf{U} + \sqrt{2D}\boldsymbol{\xi}(t), \tag{2.2b}$$

where $\mathbf{U}$ is the background flow field and β sets the intrinsic propulsion speed along the extension vector $\mathbf{w}$. The parameter τ is the relaxation timescale that drives the dimer extension toward its preferred magnitude w_0, α controls the coupling to the symmetric strain-rate tensor $\mathbf{S}$, and $\mathbf{A}$ represents the antisymmetric vorticity tensor. The term $-\ell^2 \nabla^2 \mathbf{U}$ accounts for the polar flow alignment and vanishes for an apolar (i.e., fore–aft symmetric) particle. The stochastic forcing $\boldsymbol{\xi}(t)$ is Gaussian white noise with zero mean and unit variance. The noise strength D determines the effective rotational diffusion of the dimer. Because planktonic swimmers typically have particle Reynolds numbers of order 10^{-3} and Stokes numbers of order 10^{-6}, unsteady hydrodynamic effects such as the Basset–Boussinesq history force are negligible in this regime (Jaganathan *et al.* 2023).

In addition to their advective and orientational dynamics, the particles undergo reproduction and death processes. At each time step, the distance between every pair of particles is evaluated. When two particles approach within a threshold distance d_{th}, they reproduce by creating a new particle located at the mean position of the parent pair, $(\mathbf{X}_i + \mathbf{X}_j)/2$. In single-gender cases, reproduction is permitted between any particles. In two-gender cases, reproduction is permitted only between particles of opposite gender. If a particle lies within d_{th} of multiple compatible neighbors, it may reproduce with each

Domain	q_0	F_0	ν	γ	Δt
512^2	3 m^{-1}	0.1 $\mathrm{m/s}^2$	5×10^{-6} m^2/s	0.01 s^{-1}	0.001 s

TABLE 1. Pseudospectral DNS parameters.

β	ℓ/w_0	w_0	τ	d_{th}	λ
0.175 s^{-1}	1	5×10^{-4} m	1 s	2×10^{-5} m	0.05 s^{-1}

TABLE 2. Parameters governing particle dynamics.

of them, giving rise to multiple offspring during the same time step. Alongside reproduction, particles are removed stochastically according to a constant death rate λ, such that each particle is eliminated with probability $\lambda\Delta t$ in a given time interval Δt.

3. Numerical scheme

The fluid equations (Eq. (2.1)) are solved using a pseudospectral method on a 2π periodic square domain with dealiasing by the 2/3 rule (Boffetta & Ecke 2012), using the parameters listed in Table 1. These parameters create an ambient turbulent flow with root-mean-square velocity gradient $\kappa = \sqrt{\nabla\mathbf{U} : \nabla\mathbf{U}} = 0.8454\ \mathrm{s}^{-1}$. The particles are modeled as point particles that do not exert feedback on the flow (one-way coupling), using the parameters listed in Table 2. Their translational dynamics are fully Lagrangian and are advanced according to Eq. (2.2).

Time advancement of both fluid and particle equations is performed using a fourth-order Runge–Kutta (RK4) algorithm with fixed time step Δt. The velocity field $\mathbf{U}$, together with its gradients $\nabla\mathbf{U}$ and $\nabla^2\mathbf{U}$, are interpolated to the particle positions using bilinear interpolation. Particle reproduction and death processes are evaluated at each RK4 substep to ensure consistency with the dynamics. The system starts with 50,000 particles, and the number of particles is capped at 100,000. Simulation terminates when the particle number reaches its maximum. All simulations are implemented in C, with fast Fourier transforms carried out using the FFTW library.

4. Analysis

To quantify emergent dynamics, we extracted three complementary measures from the simulations. An additional survival count was obtained by subtracting the instantaneous population of active particles from that of a corresponding control run without mating interactions, thereby isolating the net reproductive contribution. The density fluctuations were evaluated by discretizing the $2\pi \times 2\pi$ domain into 314×314 cells, such that the initial condition corresponded to 0.5 particles per cell on average. The local deviation of occupancy from this homogeneous baseline was squared and averaged across all cells, yielding a time-resolved measure of number–density variance. The Fano factor of occupancy (F) was calculated by dividing the number–density variance by the mean of the cell counts. For a Poisson (random) distribution, $F = 1$, and values $F > 1$ indicate clustering. Particle collisions were identified by coarse-graining trajectories into grid boxes of

size 512×512. Within each box, all pairwise velocity vectors were compared, and linear extrapolation was used to determine whether the trajectories intersected within a short time window Δt. Colliding indices were flagged and tracked separately from the surviving population. Together, these measures provide a quantitative basis for comparing survival, aggregation, and encounter rates across parameter regimes.

5. Results and discussion

5.1. *Same-gender mating in two-dimensional turbulence*

We first examine the case of same-gender mating in two-dimensional turbulence. Figure 1(a–f) shows particle distributions overlaid with the vorticity field of the background turbulence, scaled by the root-mean-square velocity gradient. Figure 1(a–c) shows snapshots at $t/\tau = 0$, and Figure 1(d–f) shows snapshots at $t/\tau = 32$. In Figure 1(a,d), mating is disabled with $\beta/\kappa = 207$, a regime where caustic formation is expected; in Figure 1(b,e), mating is enabled with the same $\beta/\kappa = 207$; and in Figure 1(c,f), mating is enabled with $\beta/\kappa = 2070$, a regime where caustic formation is not expected (Chajwa *et al.* 2023). In Figure 1(d), a thin band of active particles forms in the region of caustics. In Figure 1(e), a dense band of active particles forms as mating occurs within regions of caustics, whereas no such band develops in Figure 1(f), consistent with the absence of caustics.

Figure 1(g) quantifies the survival count as a function of normalized time t/τ for three cases: no mating, mating with $\beta/\kappa = 207$, and mating with $\beta/\kappa = 2070$. Populations without mating collapse, as expected. When mating is allowed in the caustic regime, survival increases sharply after $t/\tau \approx 30$. In contrast, mating without caustic formation does not sustain the population, which again collapses. These observations demonstrate that caustic formation is essential for sustaining mating in turbulence.

To probe this link further, Figure 1(h,i) compares additional survival counts (relative to the no-mating case) with the Fano factor. For the caustic case ($\beta/\kappa = 207$; Figure 1(h)), the Fano factor rises as caustics develop and coincides with an increase in survival count. For the non-caustic case ($\beta/\kappa = 207$; Figure 1(i)), the Fano factor remains close to one and the survival gain remains negligible (<1 of the initial population size).

To evaluate this connection further, Figure 2 shows collision maps at $t/\tau = 32$ for two mating regimes. In the caustic case ($\beta/\kappa = 207$; Figure 2(a)), red particles colocalize with the thick bands within the caustic structure shown in Figure 1(e). In the non-caustic case ($\beta/\kappa = 2070$; Figure 2(b)), collisions are sparse and scattered. The visual correspondence between caustic bands and collision zones provides direct evidence that caustics not only concentrate particles but also localize encounters.

Taken together, Figures 1 and 2 suggest a mechanistic picture, namely one in which caustics create transient, high-density bands that elevate collision frequency and thereby amplify mating success. Without caustics, particles are scattered, encounters remain rare, and populations collapse. Prior work identified thresholds for caustic formation in turbulent flows (Chajwa *et al.* 2023), but here we demonstrate a direct biological consequence—successful population growth depends on caustics. This coupling between a fluid-mechanical singularity and reproductive dynamics is, to our knowledge, the first demonstration that caustic formation can govern mating success in active particles suspended in turbulence.

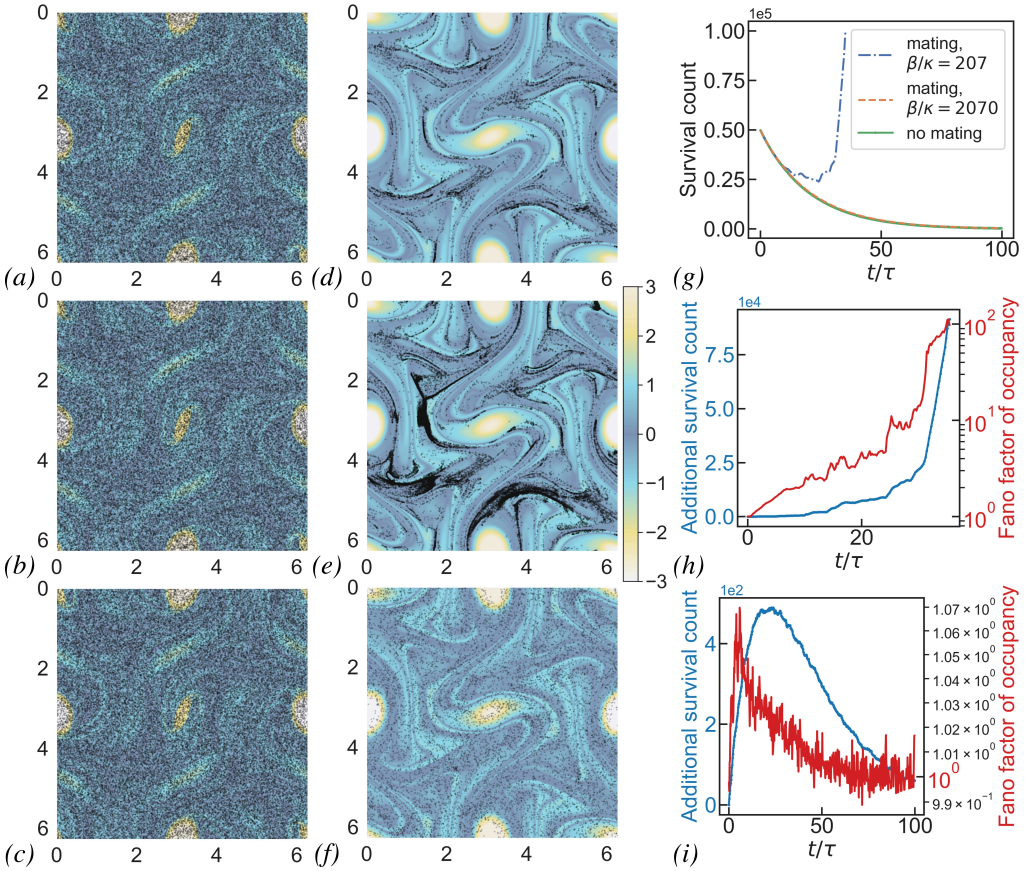

FIGURE 1. Active caustics with same-gender mating. (a–c) Initial particle distributions at $t/\tau = 0$. (d–f) Particle distributions at $t/\tau = 32$. The blue–yellow color bar represents the vorticity magnitude in the ambient turbulent flow scaled by the root-mean-square velocity gradient, and black speckles mark the geometric centers of active particles. (a,d) No mating with $\beta/\kappa = 207$, where caustic formation is expected. (b,e) Mating enabled with $\beta/\kappa = 207$, where caustic formation is expected. (c,f) Mating enabled with $\beta/\kappa = 2070$, where caustic formation is not expected, consistent with Chajwa *et al.* (2023). (g) Survival count as a function of t/τ for three cases: no mating, mating with $\beta/\kappa = 207$, and mating with $\beta/\kappa = 2070$. Populations with no mating or no caustic formation collapse, whereas populations with mating and caustic formation can achieve rapid population growth. (h) Additional survival count (relative to the no-mating case) compared with the Fano factor of occupancy for the caustic regime ($\beta/\kappa = 207$). (i) Additional survival count compared with the Fano factor of occupancy for the non-caustic regime ($\beta/\kappa = 2070$). A large Fano factor (indicative of caustic formation) corresponds to a greater additional survival count.

5.2. *Cross-gender mating in two-dimensional turbulence*

We next examine the case of cross-gender mating in two-dimensional turbulence. Figure 3(a–d) shows particle distributions at $t/\tau = 0$ (Figure 3(a,b)) and $t/\tau = 33$ (Figure 3(c,d)), overlaid with the vorticity field of the background turbulence. In Figure 3(a,c), the motility of the two genders differs by 10% ($\beta_0/\kappa = 183$, $\beta_1/\kappa = 207$), so that both genders form caustics individually but the structures are mismatched. In Figure 3(b,d), the two genders have identical motility ($\beta_0/\kappa = \beta_1/\kappa = 207$), producing caustics that overlap and match. At $t/\tau = 33$, mismatched caustics yield adjacent but segregated thin

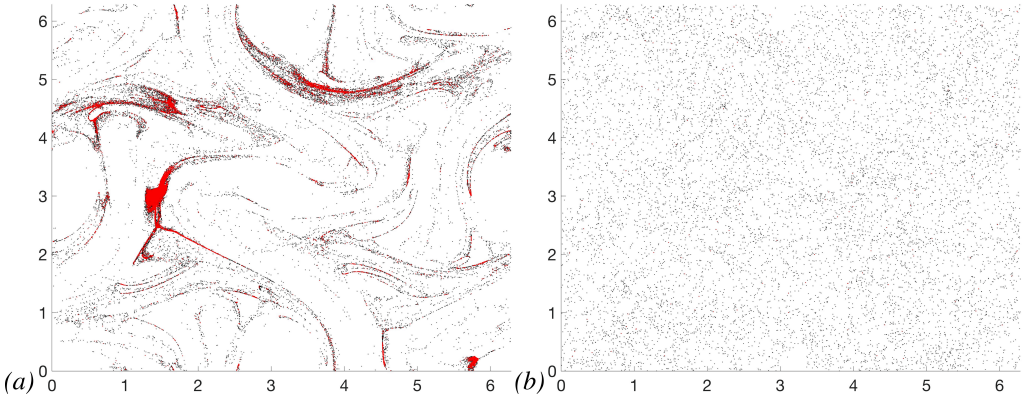

FIGURE 2. Collision maps for same-gender mating. Particle distributions at $t/\tau = 32$. (a) $\beta/\kappa = 207$, where caustic formation is expected. (b) $\beta/\kappa = 2070$, where caustic formation is not expected. Black speckles mark particles that did not collide, and red speckles indicate particles that underwent collisions.

bands of each gender (Figure 3(c)), whereas matched caustics generate coincident bands containing both genders (Figure 3(d)).

Figure 3(e) presents the survival count as a function of normalized time t/τ for three cases: no mating, mating with mismatched caustics, and mating with matched caustics. Populations without mating collapse, as expected. A similar collapse occurs when caustics are mismatched between genders, even though each gender individually forms caustics. By contrast, when caustics are matched, the population begins to grow rapidly after $t/\tau \approx 50$ and eventually reaches levels comparable to the same-gender caustic case. This result highlights that successful mating requires not only caustic formation but also synchrony between the caustics of both genders.

Figure 3(f,g) quantifies the survival count relative to the no-mating case, along with the Fano factor, as a function of normalized time t/τ. In the mismatched case (Figure 3(e)), the Fano factor transiently increases as caustics form for each gender, but because the caustics are not aligned, the survival count collapses and the Fano factor also decreases. In the matched case (Figure 3(f)), the Fano factor rises in synchrony with the additional survival count. Population growth initiates slightly later than in the same-gender case, but once underway, the survival trajectory becomes comparable, confirming that overlapping caustics between genders are required for sustained population growth.

To provide further evidence of this mechanism, Figure 4 shows collision maps at $t/\tau = 33$. In the mismatched case (Figure 4(a)), each gender forms its own caustic band, but the bands are offset and very few collisions occur between genders. In the matched case (Figure 4(b)), the red markers align with the overlapping caustic band, indicating widespread collisions within shared structures. The contrast between Figure 4(a) and Figure 4(b) demonstrates that while caustics may form independently, only their spatial overlap ensures high encounter rates.

Taken together, Figures 3 and 4 indicate that mating between two genders in turbulence requires not only caustic formation but also a synchrony of caustics across genders. Overlapping caustics create dense, mixed bands where collisions are frequent, enabling population growth. Without overlap, encounters remain rare and populations collapse despite the presence of caustics in each gender. This result shows that a singular structure of turbulent transport emerges as a determinant of mating success. While demonstrated

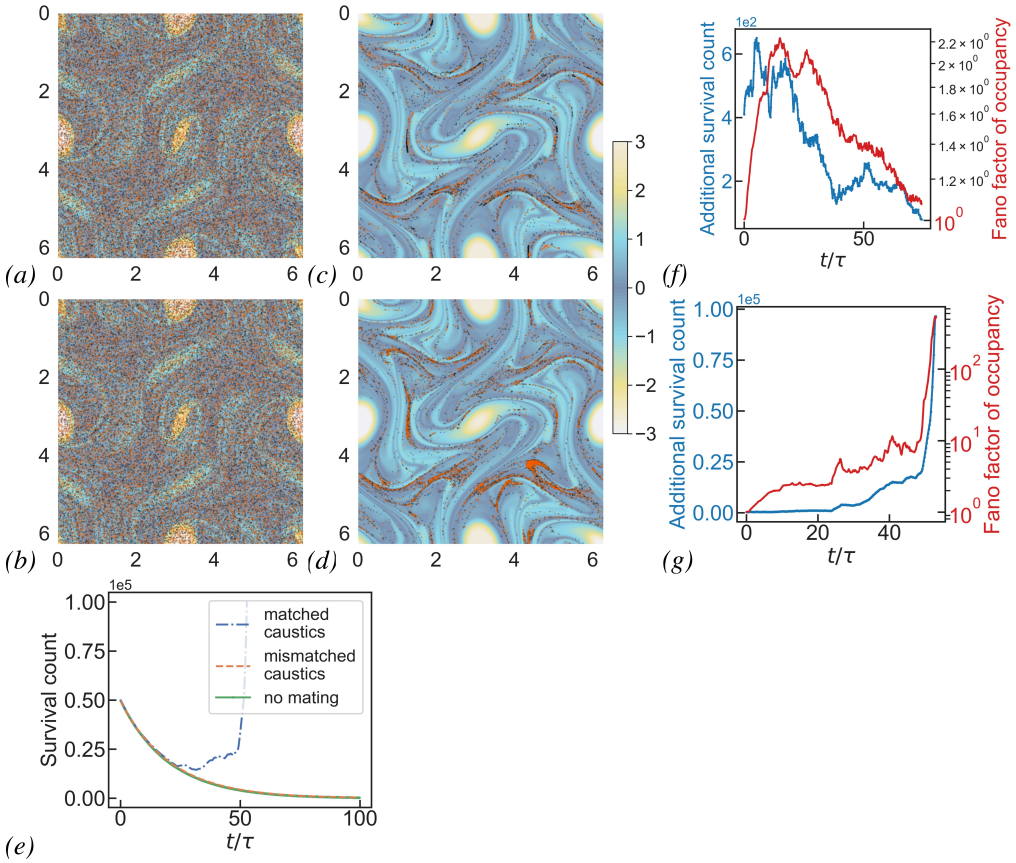

FIGURE 3. Active caustics with mating between different genders. (a,b) Initial particle distributions at $t/\tau = 0$. (c,d) Particle distributions at $t/\tau = 33$. The blue–yellow color bar represents the vorticity magnitude in the ambient turbulent flow scaled by the root-mean-square velocity gradient. Black and orange speckles mark the geometric centers of active particles of two different genders. (a,c) The motility of the two genders differs by 10%, so that each gender forms caustics in turbulence but their caustics are mismatched ($\beta_0/\kappa = 183$, $\beta_1/\kappa = 207$). (b,d) The two genders have identical motility, forming caustics that match and overlap ($\beta_0/\kappa = \beta_1/\kappa = 207$). (e) Survival count as a function of t/τ for three cases: no mating, mating with matched caustics, and mating with mismatched caustics. Populations with no mating or with mismatched caustics collapse, whereas populations with mating and matched caustics can achieve rapid population growth. (f) Additional survival count (relative to the no-mating case) compared with the Fano factor for mismatched caustics ($\beta_0/\kappa = 183$, $\beta_1/\kappa = 207$). (g) Additional survival count compared with the Fano factor for matched caustics ($\beta_0/\kappa = \beta_1/\kappa = 207$).

here in a simplified two-gender model, the principle suggests a broader role for caustic synchrony in encounter-driven processes across biological suspensions.

One implication of our results is that, in planktonic sexual reproduction, many species exhibit little or no sexual dimorphism in body size or swimming speed, with mating types distinguished only at the molecular level. For example, the green alga *Chlamydomonas reinhardtii* has two mating types that are morphologically and behaviorally indistinguishable under light microscopy and swim at comparable speeds (Seed & Tomkins 2018). Our findings suggest that turbulent flow, caustic formation, and the requirement of physical encounters for mating may impose evolutionary pressure against anisogamy in plankton,

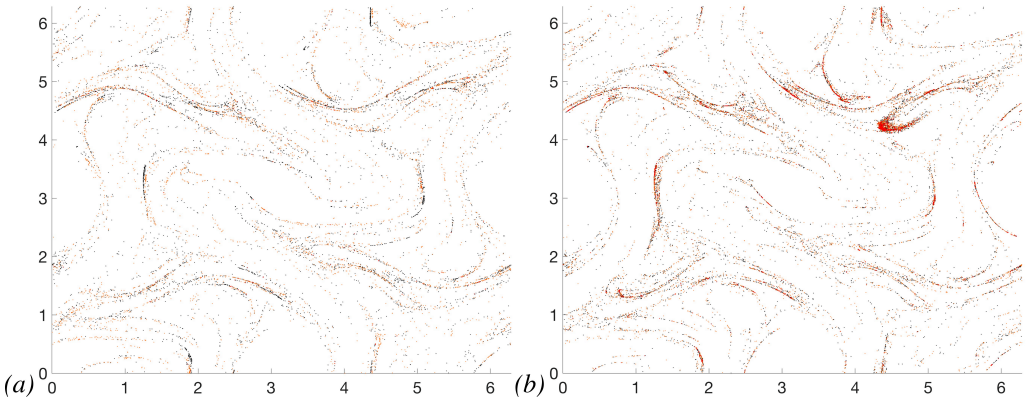

FIGURE 4. Collision maps for cross-gender mating. Particle distributions at $t/\tau = 33$. (a) $\beta_0/\kappa = 183$ and $\beta_1/\kappa = 207$, where caustics of the two genders are mismatched. (b) $\beta_0/\kappa = \beta_1/\kappa = 207$, where caustics of the two genders are matched. Black and orange speckles mark particles of two genders that did not collide, and red speckles indicate particles that underwent collisions. Matched caustics yield more widespread collisions, whereas mismatched caustics limit encounter rates.

where gametes differ in size or form. The evolution of anisogamy or sexual dimorphism in planktonic species may therefore require mechanisms that restore overlap of caustics, such as the formation of inertial caustics by immotile eggs versus the formation of active caustics by motile sperm, or the development of sensory and behavioral adaptations to overcome the encounter constraints of turbulence, as observed in copepods (Michalec *et al.* 2020).

A sensitivity analysis with respect to particle size or motility strength would likely shift the system between the inertial and active caustic regimes. Smaller or lighter particles, with lower Stokes numbers, would experience weaker inertial effects and rely primarily on activity-driven caustics, whereas larger or denser ones would form inertial caustics dominated by particle–flow slip. Regardless of the regime, our results predict that successful reproduction requires overlap of caustics between mating types, suggesting that this overlap is a criterion for population persistence.

Understanding how caustics structure encounters thus offers a framework for linking turbulence to ecological and evolutionary outcomes. Such insight may aid coral preservation, where turbulent flows regulate gamete encounters (Davis *et al.* 2021), and could also inform strategies to suppress harmful algal blooms by disrupting the fluid-mechanical conditions that favor their reproduction. Future work can extend these results by exploring mixed inertial and active caustics and mapping reproduction success across parameter regimes in a phase diagram. Experimental observations of mating in controlled turbulent flows will also be essential to test these predictions and connect them with biological systems.

6. Conclusions

We have shown that caustic formation in turbulence governs the mating success of active particles. In the same-gender case, caustics concentrate particles into transient bands that elevate the rate of collisions and enable rapid population growth, whereas populations collapse in their absence. In the cross-gender case, successful reproduction requires not only caustics but also synchrony between genders, and only overlapping caustics yield

sufficient encounters for growth. These results demonstrate that a singular structure of turbulent transport can determine biological outcomes, linking fluid mechanics directly to reproductive dynamics. The principle suggests that caustics may shape the evolution of mating strategies in planktonic species, where the probability of an encounter is constrained by turbulence. By establishing caustic overlap as a prerequisite for reproductive success, our work introduces a new perspective on how microscale fluid mechanics can influence large-scale ecological and evolutionary patterns.

7. Acknowledgment

The support of ONR to CTR under grant N000142312833 is gratefully acknowledged.

REFERENCES

Bagøien, E. & Kiørboe, T. 2005 Blind dating—mate finding in planktonic copepods. I. Tracking the pheromone trail of *Centropages typicus*. *Mar. Ecol. Prog. Ser.* **300**, 105–115.

Berg, H. C. & Purcell, E. M. 1977 Physics of chemoreception. *Biophys. J.* **20**, 193–219.

Bhatnagar, A., Pandey, V., Perlekar, P. & Mitra, D. 2022 Rate of formation of caustics in heavy particles advected by turbulence. *Philos. Trans. London Ser. A* **380**, 20210086.

Boffetta, G. & Ecke, R. E. 2012 Two-dimensional turbulence. *Annu. Rev. Fluid Mech.* **44**, 427–451.

Bryan, A. K., Goranov, A., Amon, A. & Manalis, S. R. 2010 Measurement of mass, density, and volume during the cell cycle of yeast. *Proc. Natl. Acad. Sci. USA* **107**, 999–1004.

Chajwa, R., Rajarshi, Ramaswamy, S. & Govindarajan, R. 2023 Active caustics. arXiv:2310.01829 [cond-mat.soft].

Davis, K. A., Pawlak, G. & Monismith, S. G. 2021 Turbulence and coral reefs. *Annu. Rev. Mar. Sci.* **13**, 343–373.

Evans, R., Dal Poggetto, G., Nilsson, M. & Morris, G. A. 2018 Improving the interpretation of small molecule diffusion coefficients. *Anal. Chem.* **90**, 3987–3994.

Frenkel, J., Vyverman, W. & Pohnert, G. 2014 Pheromone signaling during sexual reproduction in algae. *Plant J.* **79**, 632–644.

Guasto, J. S., Rusconi, R. & Stocker, R. 2012 Fluid mechanics of planktonic microorganisms. *Annu. Rev. Fluid Mech.* **44**, 373–400.

Gustavsson, K., Meneguz, E., Reeks, M. & Mehlig, B. 2012 Inertial-particle dynamics in turbulent flows: caustics, concentration fluctuations and random uncorrelated motion. *New J. Phys.* **14**, 115017.

Jaganathan, D., Prasath, S. G., Govindarajan, R. & Vasan, V. 2023 The Basset–Boussinesq history force: its neglect, validity, and recent numerical developments. *Front. Phys.* **11**, 1167338.

Kiørboe, T. 2008 A mechanistic approach to plankton ecology. *ASLO Web Lect.* **1**, 1–91.

Kiørboe, T. & Bagøien, E. 2005 Motility patterns and mate encounter rates in planktonic copepods. *Limnol. Oceanogr.* **50**, 1999–2007.

Menden-Deuer, S. 2006 An integrated model simulation and empirical laboratory on biological encounter rates. *Oceanography* **19**, 185–189.

Michalec, F.-G., Fouxon, I., Souissi, S. & Holzner, M. 2020 Efficient mate finding in planktonic copepods swimming in turbulence. *eLife* **9**, e62014.

Nelson, G., Strain, A., Isu, A., Rahnama, A., Wakabayashi, K.-I., Melvin, A. T. & Kato, N. 2023 Cells collectively migrate during ammonium chemotaxis in *Chlamydomonas reinhardtii*. *Sci. Rep.* **13**, 10781.

Papoutsakis, A. & Gavaises, M. 2020 A model for the investigation of the second-order structure of caustic formations in dispersed flows. *J. Fluid Mech.* **892**, A4.

Pumir, A. & Wilkinson, M. 2016 Collisional aggregation due to turbulence. *Annu. Rev. Condens. Matter Phys.* **7**, 141–170.

Seed, C. E. & Tomkins, J. L. 2018 Positive size-speed relationships in gametes and vegetative cells of *Chlamydomonas reinhardtii*: implications for the evolution of sperm. *Evolution* **72**, 440–452.

Segall, J. E., Block, S. M. & Berg, H. C. 1986 Temporal comparisons in bacterial chemotaxis. *Proc. Natl. Acad. Sci. USA* **83**, 8987–8991.

Seuront, L. & Stanley, H. E. 2014 Anomalous diffusion and multifractality enhance mating encounters in the ocean. *Proc. Natl. Acad. Sci. USA* **111**, 2206–2211.

Yen, J. & Lasley, R. 2010 Chemical communication between copepods: finding the mate in a fluid environment. In *Chemical Communication in Crustaceans*, ed. T. Breithaupt & M. Thiel, pp. 177–197. Springer.